Publishing House
AKAPIT

COMPUTER METHODS IN MATERIALS SCIENCE

Informatyka w Technologii Materiałów

Vol. 13, 2013, No. 2

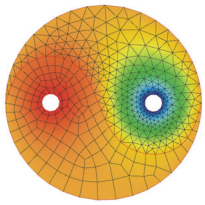

FIRST PRINCIPLES PHASE DIAGRAM CALCULATIONS FOR THE CdSe-CdS WURTZITE, ZINCBLENDE AND ROCK SALT STRUCTURES

ANDRZEJ WOŹNIAKOWSKI[1], JÓZEF DENISZCZYK[1], OMAR ADJAOUD[2,4], BENJAMIN P. BURTON[3]

[1] Institute of Materials Science, University of Silesia, Bankowa 12, 40-007 Katowice, Poland
[2] GFZ German Research Centre for Geosciences, Section 3.3, Telegrafenberg, 14473 Potsdam, Germany
[3] Ceramics Division, Materials Science and Engineering Laboratory, National Institute of Standards and Technology, Gaithersburg, Maryland 20899-8520, USA
[4] Present address: Technische Universität Darmstadt, Fachbereich Material- und Geowissenschaften, Fachgebiet Materialmodellierung, Petersenstr. 32, D-64287 Darmstadt, Germany
**Corresponding author: andrzej.wozniakowski@us.edu.pl*

Abstract

The phase diagrams of $CdSe_{1-x}S_x$ alloys were calculated for three different crystal structure types: wurtzite (B4); zinc-blende (B3); and rocksalt (B1). *Ab initio* calculations of supercell formation energies were fit to cluster expansion Hamiltonians, and Monte Carlo simulations were used to calculate finite temperature phase relations. The calculated phase diagrams have symmetric miscibility gaps for B3 and B4 structure types and a slightly asymmetric diagram for B1 structure. Excess vibrational contributions to the free energy were included, and with these, calculated consolute temperatures are: 270 K for B4; 300 K for B3; and 270 K for B1. Calculated consolute temperatures for all structures are in good quantitative agreement with experimental data.

Key words: clamping, groove rolling, FEM

1. INTRODUCTION

The cadmium chalcogenide $CdSe_{1-x}S_x$ semiconducting alloy is characterized by a variable direct band gap which can be tuned by alloying, from 1.72 eV for CdSe to 2.44 eV for CdS. Because of excellent properties Cd(S,Se) is used in optoelectronic devices, photoconductors, gamma ray detectors, visible-light emitting diodes, lasers and solar cells (Xu et al., 2009; and references cited therein). $CdSe_{1-x}S_x$ solid solutions have attracted great interest in recent years from both experimental and theoretical points of view (Xu et al., 2009; Mujica et al., 2003; Wei & Zhang, 2000; Banerjee et al., 2000; Tolbert & Alivisatos, 1995; Hotje et al., 2003, Deligoz et al., 2006).

It is known that CdS and CdSe occur at normal conditions both in the wurtzite and metastable zinc-blende structures. (Mujica et al., 2003; Madelung et al., 1982). Depending on the growth conditions, the CdSe (CdS) can be synthesized in the B4, or in the metastable B3-type structure either by molecular-beam epitaxy, or by controlling the growth temperature (Wei & Zhang, 2000). The equilibrium zinc-blende structure is observed in CdS nanostructures (Banerjee et al., 2000). Under high pressure, both B3 and B4 structures convert to the denser rocksalt-

 ISSN 1641-8581

structure phase (Mujica et al., 2003; Tolbert & Alivisatos, 1995; Hotje et al., 2003).

Recent measurements of formation enthalpies (ΔH_f) for CdS_xSe_{1-x} B4-type solid solutions, reported by Xu et al. (2009), indicated that within experimental error $\Delta H_f = 0$ at 298 K. This may indicate that, at least above room temperature, that CdS and CdSe form an ideal solution in the B4- structure-type; despite differences in molar volume ($V_{mol,CdSe}$ = 33.727 cc/mol, $V_{mol,CdS}$ = 29.934 cc/mol, Davies, 1981) and anion radii (R_{CdSe} = 1.91 Å, R_{CdS} = 1.84 Å, Jug & Tikhomirov, 2006) (Xu et al., 2009). These measurements did not show the presence of a miscibility gap above 298 K, i.e. indicating that either: 1) the blocking temperature for Se/S diffusion is above T_C; or 2) the consolute temperature for CdS_xSe_{1-x} in B4 structure must be below room temperature. The *T-x* phase diagram of the CdSe-CdS system was the subject of theoretical *ab initio* studies (Ouendadji et al., 2010; Breidi, 2011; Lukas et al., 2007). In both cases (B3 and B4), only formation energies (at x = 0, 0.25, 0.5, 0.75 and 1.0) were considered, while excess vibrational free energy contributions were neglected. In Ref. (Ouendadji et al., 2010) only B3 structure was investigated, while in (Breidi, 2011) phase diagrams for both B3 and B4 structures were determined. Both studies predict miscibility gaps. For the B3-type structure the consolute temperatures (T_C) reported by Ouendadji et al. (2010) and Breidi (2011) are: T_C = 315 K and 228 K, respectively. Both predicted consolute temperatures differ from the critical temperature (T_C = 298 K) reported by Xu et al. (2009). The difference between T_C as calculated by Ouendadji et al., (2010) and Breidi (2011) originates from the different *ab initio* computational setup, and different choices of supercells for which formation energies were calculated (this difference indicates that the sets of formation energies for at least one of these calculations, and probably both, are based on sets of formation energies that are too small to yield *converged* effective Hamiltonians). For the B4-type structure Breidi (2011) reports T_C = 225 K < T_C = 228 K for the B3 structure.

The aim of this study is to compare *well converged* calculations of CdSe-CdS phase diagrams in all three crystal structure types: B1, B3 and B4. Both configurational and excess vibrational contributions to the free energy are considered. Sufficiently large sets of formation energies are used, that one can have reasonable confidence that calculated phase diagrams faithfully reflect density functional theory (DFT) energetics.

2. COMPUTATIONAL DETAILS

Calculations of formation energies, defined as $\Delta E_f = E_{CdS_xSe_{1-x}} - xE_{CdS} - (1-x)E_{CdSe}$, were performed using the Vienna *ab initio* Simulation Package VASP (Kresse & Hafner, 1993, 1994; Kresse & Furthmüller, 1996a, 1996b) implementing the Blöchl's projector augmented wave approach (Blöchl, 1994), with the generalized gradient approximation for exchange and correlation potentials. Valence electron configurations for the pseudopotentials are: $Cd = 4d^{10}5s^2$, $Se = 4s^24p^4$ and $S = 3s^23p^4$. All calculations were converged with respect to gamma centered k-point sampling, and a plane-wave energy cutoff of 350 eV was used which yields ΔE values that are converged to within a few meV per atom. Electronic degrees of freedom were optimized with a conjugate gradient algorithm. Both cell parameters and ionic positions were fully relaxed for each superstructure of underlying B1, B3 and B4 crystal structures.

Based on the VASP results, the First Principles Phase Diagram calculations were performed with the use of Alloy Theoretic Automated Toolkit (ATAT) software package (van de Walle & Ceder, 2002a; van de Walle et al., 2002; van de Walle & Asta, 2002). The VASP calculations were used to construct cluster expansion (CE) Hamiltonian in a form of polynomial in the occupation variables: $\Delta E(\sigma) = \sum_{\alpha} m_\alpha J_\alpha \left\langle \prod_{i \in \alpha'} \sigma_i \right\rangle$ (Sanchez et al., 1984), where α is a cluster defined as a set of lattice sites, m_α denote the number of clusters that are equivalent by symmetry, summation is over all clusters α that are not equivalent by a symmetry operation and an average is taken over all clusters α′ that are equivalent to α by symmetry. The Effective Cluster Interaction (ECI) coefficients, J_α, embody the information regarding the energetics of an alloy. In our investigations the well-converged cluster expansion system required calculation of the formation energy for 30-50 ordered superstructures. The predictive power of cluster expansion is controlled by cross-validation score $CVS = \left(\frac{1}{n} \sum_{i=1}^{n} (E_i - \hat{E}_{(i)})^2 \right)^{\frac{1}{2}}$, where E_i is an *ab inito* calculated formation energy of superstructure i, while $\hat{E}_{(i)}$ represent the energy of superstructure i obtained from CE with the use of the remaining (n – 1) structural energies. The free ener-

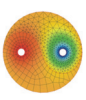

gy contributed by lattice vibrations was introduced employing the coarse-graining formalism (van de Walle & Ceder, 2002b). For each superstructure the vibrational free energy was calculated within the quasi-harmonic approximation with the application of the bond-length-dependent transferable force constant approximation (van de Walle & Ceder, 2002b).

The phase diagram calculations were performed with the use of the Monte Carlo thermodynamic integration within the semi-grand-ensemble (van de Walle & Asta, 2002). In this ensemble, for temperature (T) and chemical potentials (μ) imposed externally, the internal energy (E_i) and concentration (x_i) of constituents of an alloy with fixed number of atoms (N), are allowed to fluctuate. The thermodynamic potential ϕ (per atom) associated with the semi-grand-canonical ensemble can be defined in terms of the partition function of the system in the form presented in equation (1) (van de Walle & Asta, 2002):

$$\phi(\beta,\mu) = -\frac{1}{\beta N}\ln\left(\sum_i \exp(-\beta N(E_i - \mu x_i)\right), \quad (1)$$

where the summation is over different atomic configurations (alloy states) and $\beta = 1/(k_B T)$ (k_B is Boltzmann's constant). In the differential form (with variable T and μ) equation (1) can be rewritten in a form given by equation (2):

$$d(\beta\phi) = (\overline{E} - \mu \cdot \bar{x})\, d\beta - \beta\, \bar{x}\, d\mu\,. \quad (2)$$

where $\overline{E}$ and $\bar{x}$ are the alloy's average internal energy (calculated with the use of CE expansion) and concentration of constituents; and averaging was performed according to formula:

$$\overline{A} = \sum_i A_i \exp(-\beta N(E_i - \mu x_i)) / \sum_i \exp(-\beta N(E_i - \mu x_i))$$

Using the differential form given by equation (2) the thermodynamic potential $\phi(\beta,\mu)$ can be calculated through the thermodynamic integration described by equation (3) (van de Walle & Asta, 2002):

$$\beta_1\phi(\beta_1,\mu_1) = \beta_0\phi(\beta_0,\mu_0) + \int_{(\beta_0,\mu_0)}^{(\beta_1,\mu_1)} (E - \mu x, -\beta x)\, d(\beta,\mu) \quad (3)$$

The thermodynamic integration in (3), along a continuous path connecting points (β_0, μ_0) and (β_1, μ_1) which does not encounter the phase transition, was performed using the Monte Carlo method. The starting point (β_0, μ_0) is taken in the limit of low temperature at chemical potential stabilizing a given ground state of a system (here, the chemical potentials of end-members CdS and CdSe).

A schematic diagram of the approach is: VASP calculations of formation enthalpies and vibrational free energies for a set of superstructures → fit a cluster expansion (CE = set of effective cluster interactions, ECI) →fit effective force constants to model excess vibrational contributions → Monte Carlo thermodynamic integration → phase diagram**.** The advantage of this approach is that it is based on the parameters-free *ab initio* calculations and leads to high quality effective Hamiltonians for multicomponent systems. The CE has the limitation that it only applies to a parent structure and its superstructures.

3. RESULTS AND DISCUSSION

Using the *ab initio* (VASP) method, calculations of the ground state energy were performed for the stoichiometric compounds CdSe and CdS and for the αformation energies of many B1-, B3-, or B4-based superstructures (36 – B1, 36 – B3 and 34 – B4). All formation energies were positive, which implies that no intermediate ground state structures were predicted. The optimal number of superstructures were determined by minimizing the cross-validation score between *ab initio* computations and the cluster expansion prediction. Figure 1 shows the dependence of the CVS on the number of calculated superstructures. The convergence of CVS at values less than 1.5 meV/atom was reached for approximately 25 superstructures. Increasing further the number of superstructures results in the fluctuations of CVS with standard deviation of order of 0.1 meV/atom. The results presented in figure 1 strongly suggests convergence of the CE series.

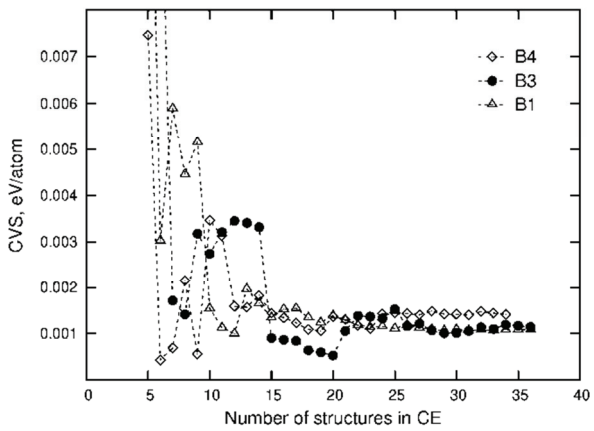

Fig. 1*. Dependence of the CVS vs number of superstructures used in the fit of CE for B1, B3 and B4 structures.*

The ECI, are plotted as functions of inter-atomic separations in figures 2. It is evident that with increasing distance, pair-ECI magnitudes decrease with oscillatory sign. The 3-body ECI, for B1 structure-type, is very small. Low values of cross validation score and decreasing magnitudes of the ECI justify truncation of CE series and discarding the larger clusters.

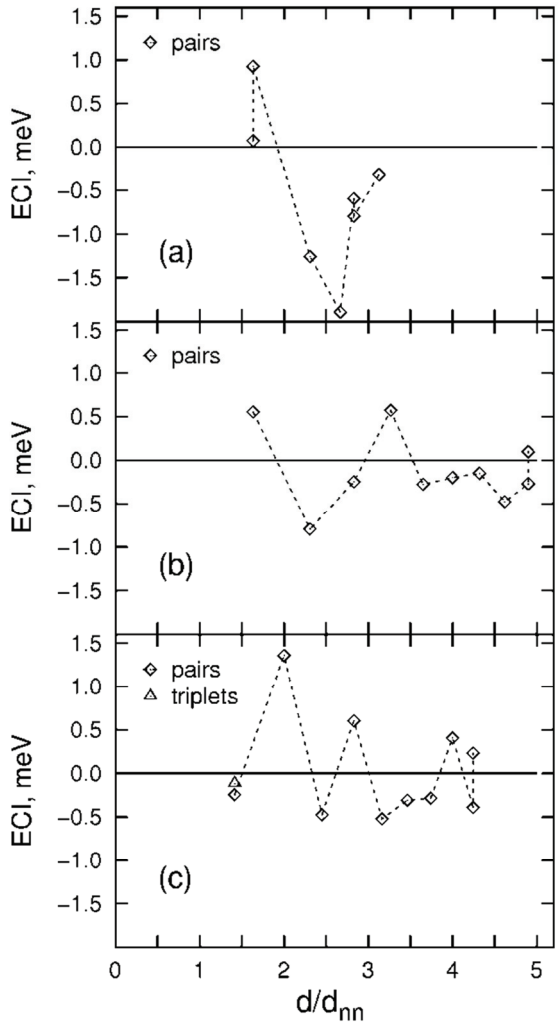

Fig. 2. *Effective cluster interactions (ECI) as functions of inter-atomic distance (d/d_{nn}) for the clusters taken into account in cluster expansion series for the B4 (figure a), B3 (figure b) and B1 (figure c) underlying crystal structures. The inter-atomic distance is expressed in units of the nearest neighbor distance (d_{nn}).*

Figures 3 are plots of the VASP-calculated supercell formation energies (ΔE_f per cation) that were used to fit the ECI in figures 2. The differences between VASP-calculated and CE-calculated are small, except for the end-members compounds CdSe and CdS in B4 structure-type; note that these differences are an order of magnitude smaller than the values ΔE_f, thus the results in figures 3, confirm the quality and predictive power of CE.

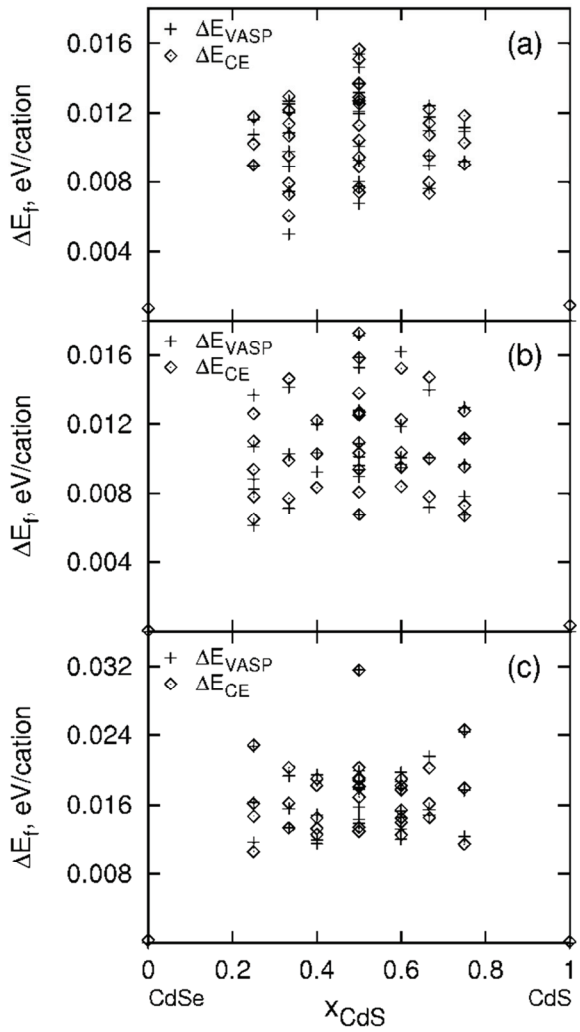

Fig. 3. *Formation energies ΔE_f calculated by VASP (cross) and fitted by cluster expansion (CE) for B4 (figure a), B3 (figure b) and B1 (figure c) structures. Note the different scale used on vertical axis of figure c.*

Note that formation energies for B1-based supercells are about twice as large as for the wurtzite and zinc-blende structures. This correlates with the higher predicted consolute temperature when only the configurational part of free energy is taken into account.

Figures 4 are the calculated phase diagrams for the CdSe-CdS system in B1, B3 and B4 crystal structures. Temperature independent ECI were used to calculate the lower solvii in (a) and (b) and the upper curve in (c) (dash lines). Temperature dependent ECI, which imply the inclusion of excess vibrational contributions to the free energy, yield the results which are plotted as the upper solvii in (a) and (b) and the lower solvus in (c) (solid lines). In most miscibility gap systems (Adjaoud, et al., 2009; Burton & van de Walle, 2006) the inclusion of temperature-dependent ECI leads to a *reduction* in T_C, thus the results in figures 3a and 3b, are atypical. However, detailed model studies of an effect of lattice

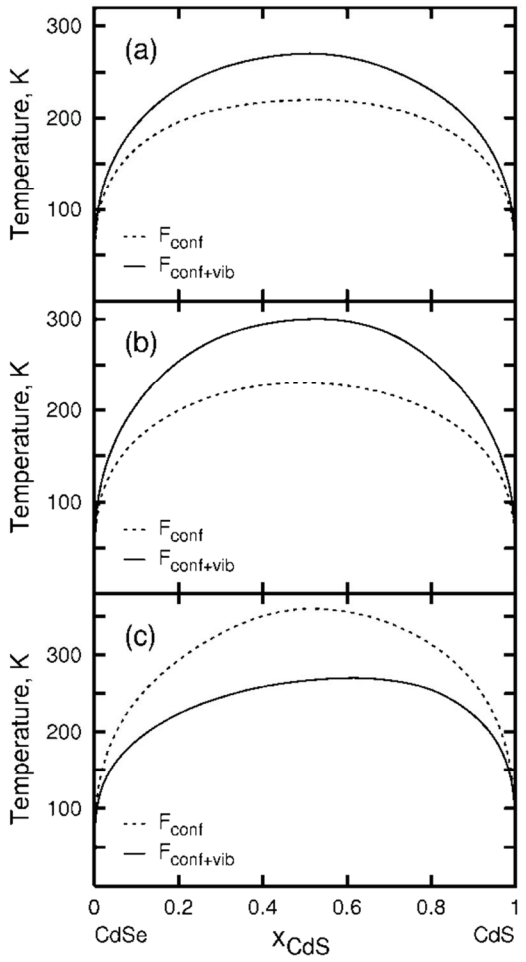

Fig. 4. *Calculated phase diagram of CdS_xSe_{1-x} alloy in B4 (figure a), B3 (figure b) and B1 (figure c). Dash and solid solvii are the phase diagrams that were calculated with temperature-independent-, and temperature-dependent ECI, respectively. The results in (a) and (b), that T-independent ECI predict lowest T_C rather than higher, is atypical.*

vibrations on the phase stabilities of substitutional alloys have shown (Garbulsky & Ceder, 1996), that inclusion of vibrations into phase-diagram modeling of miscibility gap systems can increase the consolute temperature. Furthermore, investigations of the vibrational entropy change upon order-disorder transition in Pd_3V system (van de Walle & Ceder, 2000) have shown, that the relaxation of bonds can change the sign of vibrational entropy differences as compared to the expectations based on the bond proportion model. The main feature of the calculated phase diagrams is the consolute temperature (T_C). For the B4 structure (figure 3a) the miscibility gap is symmetric with critical point (x_C, T_C) = (0.50, 220 K) when only configurational degrees of freedom are taken into account, and (x_C, T_C) = (0.50, 270 K) when temperature dependent vibrational contribution is included. For the B3 structure (figure 3b) the shape of the phase diagram does not change significantly as compared to that of B4 structure, but for the B3 structure we obtained higher consolute temperatures: 230 K and 300 K, respectively. For the B1 structure (figure 4c) the phase diagram obtained on the basis of temperature independent ECI is almost symmetric ($x_C = 0.51$). Inclusion of the vibrational contribution enhances asymmetry ($x_C = 0.61$) and reduce the critical temperature: from $T_C = 360$ K, when only formation energy is taken into account, to $T_C = 270$ K, with vibrational effects included.

4. CONCLUSIONS

A*b initio* calculations of CdSe-CdS phase diagrams for wurtzite-, zinc-blende- and rock salt structure-types were calculated by the CE-method; both without- and with excess vibrational free energy contributions (i.e. without- and with T-dependent ECI, respectively). Miscibility gaps are predicted for all three systems. When only configurational free energy is taken into account the calculated consolute temperatures are: 220 K, 230 K and 360 K for wurtzite-, zinc-blende- and rock salt structure-types, respectively. Surprisingly, the inclusion of excess vibrational contributions to the free energy *destabilizes* the B3- and B4-based solid solutions, contrary to similar studies (Burton et al., 2006), and increases the consolute temperature by 30% and 23% for wurtzite- and zinc-blende structure-types, respectively. For the rock-salt structure inclusion of vibrations reduces the consolute temperature by 25%, similarly as reported by Adjaoud, et al. (2009) for the TiC-ZrC system. Slightly above room temperature complete solid solution is possible in the zinc-blende structure. Calculated consolute temperatures for B1, B3 and B4 structure-types compare well with experimental critical temperature $T_C = 298$ K reported by Xu, et al., (2009).

REFERENCES

Adjaoud, O., Steinle-Neumann, G., Burton, B.P., van de Walle, A., 2009, First-principles phase diagram calculations for the HfC-TiC, ZrC-TiC, and HfC-ZrC solid solutions, *Phys. Rev. B*, 80, 134112-134119.

Banerjee, R., Jayakrishnan, R., Ayyub, P., 2000, Effect of the size-induced structural transformation on the band gap in CdS nanoparticles, *J. Phys. Condens. Matter*, 12, 10647-10654.

Blöchl, P. E., 1994, Projector augmented-wave method, *Phys. Rev. B*, 50, 17953-17979.

Burton, B.P., van de Walle, A., 2006, First principles phase diagram calculations for the system NaCl-KCl: The role of excess vibrational entropy, *Chem. Geo.*, 225, 222-229.

Burton, B.P., van de Walle, A., Kattner, U., 2006, First principles phase diagram calculations for the wurtzite-structure systems AlN-GaN, GaN-InN, and AlN-InN, *Journ. Appl. Phys*., 100, 113528-113534.

Breidi, A., 2011, *Temperature–pressure phase diagrams, structural and electronic properties of binary and pseudobinary semiconductors: an ab initio study*, PhD thesis, l'Université Pual Verlaine, Metz.

Davies, P.K., 1981, *Thermodynamics of solid solution formation*, PhD thesis, Arizona State University, Arizona.

Deligoz, E., Colakoglu, K., Ciftci, Y., 2006, Elastic, electronic, and lattice dynamical properties of CdS, CdSe, and CdTe, *Physica B*, 373, 124-130.

Garbulsky, G.D., Ceder, G., 1996, Contribution of the vibrational free energy to phase stability in substitutional alloys: Methods and trends, *Phys. Rev. B*,53, 8993-9001.

Hotje, U., Rose, C., Binnewies, M., 2003, Lattice constants and molar volume in the system ZnS, ZnSe, CdS, CdSe, *Sol. State Sci*., 5, 1259-1262.

Jug, K., Tikhomirov, V.A., 2006, Anion substitution in zinc chalcogenides, *J. Comput. Chem.* 27, 1088-1092.

Kresse, G., Hafner, J., 1993, *Ab initio* molecular dynamics for liquid metals, *Phys. Rev. B*, 47, 558-561.

Kresse, G., Hafner, J., 1994, *Ab initio* molecular simulation of the liquid-metal–amorphous-semiconductor transition in germanium, *Phys. Rev. B*, 49, 14251-14269.

Kresse, G., Furthmüller, J., 1996a, Efficiency of *ab-initio* total energy calculations for metals and semiconductors using a plane-wave basis set, *Comput. Mater. Sci*., 6, 15-50.

Kresse, G., Furthmüller, J., 1996b, Efficient iterative schemes for *ab initio* total-energy calculations using a plane-wave basis set, *Phys. Rev. B*, 54, 11169-11186.

Lukas, H. L., Fries, S. G., Sundman, B., 2007, *Computational Thermodynamics. The Calphad Method*, Cambridge Press, Cambridge.

Madelung, O., Schultz, M., Weiss, H., 1982, *Landolt-Bornstein Numerical Data and Functional Relationships in Science and Technology*, group III, 17b, Springer-Verlag, Berlin.

Mujica, A., Rubio, A., Munoz, A., Needs, R.J., 2003, High pressure phases of group IV, II-V and II-VI compounds, *Rev. Mod. Phys*., 75, 863-912.

Ouendadji, S., Ghemid, S., Meradji, H., El Haj Hassan, F., 2010, Density functional study of $CdS_{1-x}Se_x$ and $CdS_{1-x}Te_x$ alloys, *Comput. Mater. Sci*., 48, 206-211.

Sanchez, J.M., Ducastelle, F., Gratias, D., 1984, Generalized cluster description of multicomponent systems, *Physica A*, 128, 334-350.

Tolbert, S.H., Alivisatos, A.P., 1995, The wurtzite to rock salt transformation structural transformation in CdSe nanocrystals under high pressure, *J. Chem. Phys*., 102, 4642-4656.

van de Walle, A., Ceder, G., 2000, First-principles computation of the vibrational entropy of ordered and disordered Pd_3V, *Phys. Rev. B*, 61, 5972-5978.

van de Walle, A., Ceder, G., 2002a, Automating first-principles phase diagram calculations, *J. Phase Equilib*., 23, 348-359.

van de Walle, A., Asta, M., Ceder, G., 2002, The alloy theoretic automated toolkit: A user guide, *Calphad*, 26, 539-553.

van de Walle, A., Asta, M., 2002, Self-driven lattice-model Monte Carlo simulations of alloy thermodynamic, *Modelling Simul. Mater. Sci. Eng*., 10, 521-538.

van de Walle, A., Ceder, G., 2002b, The effect of lattice vibrations on substitutional alloy thermodynamics, *Rev. Mod. Phys*., 74, 11-45.

Wei, S.-H., Zhang, S.B., 2000, Structure stability and carier localization in CdX(X=S, Se, Te) semiconductors, *Phys. Rev. B*, 62, 6944-6947.

Xu, F., Ma, X., Kauzlarich, S.M., Navrotsky, A., 2009, Enthalpies of formation of CdS_xSe_{1-x} solid solutions, *J. Mater. Res*., 24, 1368-1374.

OBLICZENIA Z PIERWSZYCH ZASAD DIAGRAMÓW FAZOWYCH DLA PSEUDOBINARNEGO SYSTEMU CdSe-CdS KRYSTALIZUJĄCEGO W SIECIACH WURCYTU, BLENDY CYNKOWEJ ORAZ SOLI KAMIENNEJ

Streszczenie

Półprzewodnikowe związki Cd(Se,S) oraz ich stopy charakteryzują się szeroką bezpośrednią przerwą energetyczną i dlatego mogą być przydatne w urządzeniach optoelektronicznych, światłoczułych, detektorach promieniowania gamma, diodach elektroluminescencyjnych, laserach oraz ogniwach słonecznych. Ze względu na możliwość atrakcyjnych zastosowań półprzewodnikowe stopy $CdSe_{1-x}S_x$ są w ostatnich latach przedmiotem rozważań teoretycznych oraz intensywnych badań doświadczalnych.

Związki Cd(Se,S) w warunkach normalnych krystalizują w heksagonalnej strukturze wurcytu (B4) oraz metastabilnej, ściennie centrowanej strukturze blendy cynkowej (B3). Pod wpływem wysokiego ciśnienia struktury B4 oraz B3 zmieniają swoją formę krystaliczną i przekształcają się w gęstszą, ściennie centrowaną strukturę soli kamiennej (B1).

Celem niniejszej pracy jest przeprowadzenie obliczeń diagramów fazowych oraz wyznaczenie krytycznej temperatury mieszalności dla stopów $CdSe_{1-x}S_x$ krystalizujących w strukturach B4, B3 oraz B1.

Diagramy fazowe zostały wyznaczone na podstawie potencjałów termodynamicznych obliczonych metodą całkowania termodynamicznego Monte Carlo. Zrealizowany proces obliczeń wskazuje na występowanie luk mieszalności w całym zakresie koncentracji $CdSe_{1-x}S_x$ dla wszystkich rozpatrywanych sieci krystalicznych. Rezultaty uzyskane dla struktur sieci B4 oraz B3 charakteryzują się symetrycznymi lukami mieszalności. W przypadku struktur sieci B1 luka mieszalności wykazuje lekko asymetryczny charakter. Wyznaczone krytyczne temperatury mieszalności wynoszą 270 K, 300 K, 270 K odpowiednio dla struktur sieci B4, B3 i B1. W obliczeniach uwzględniono efekt drgań sieci, a uzyskane rezultaty wykazują dobrą zgodność z dostępnymi w literaturze danymi eksperymentalnymi.

Received: October 29, 2012
Received in a revised form: December 3, 2012
Accepted: December 8, 2012